IEEE Access
Multidisciplinary | Rapid Review | Open Access Journal

Received 10 July 2024, accepted 1 August 2024, date of publication 7 August 2024, date of current version 19 August 2024.

Digital Object Identifier 10.1109/ACCESS.2024.3440039

RESEARCH ARTICLE

Magnetic Field Mitigation in Dynamic Wireless Power Transfer Systems by Double Sided LCC Compensation

TOMMASO CAMPI[1], SILVANO CRUCIANI[2], FRANCESCA MARADEI[1], (Senior Member, IEEE), AND MAURO FELIZIANI[3], (Senior Member, IEEE)

[1]Department of Astronautics, Electrical and Energetic Engineering, Sapienza University of Rome, 00184 Rome, Italy
[2]Department of Industrial Engineering, Tor Vergata University of Rome, 00133 Rome, Italy
[3]Department of Industrial and Information Engineering and Economics, University of L'Aquila, 67100 L'Aquila, Italy

Corresponding author: Tommaso Campi (tommaso.campi@uniroma1.it)

ABSTRACT This paper deals with the mitigation of magnetic field emission in dynamic wireless power transfer (DWPT) systems. DWPTs are used to charge electric vehicles (EVs) in motion along electrified roads. A critical aspect of these systems is the magnetic field that must be compliant with regulation limits. In this work, a formulation for fine tuning of the LCC compensation is adopted to control magnetic field emission while maintaining high electrical performances and without varying the input impedance of the system. The numerical results demonstrate the proposed approach's effectiveness in mitigating magnetic field emissions to comply with electromagnetic field (EMF) safety limits, while also improving power transfer efficiency.

INDEX TERMS Battery charging, dynamic wireless power transfer (DWPT), electric vehicle (EV), electromagnetic compatibility (EMC), electromagnetic field (EMF) safety, LCC compensation, magnetic fields, wireless power transfer (WPT).

I. INTRODUCTION

With the growing popularity of electric vehicles (EVs), the need for efficient and convenient charging solutions is fundamental. Dynamic wireless power transfer (DWPT) offers a promising approach to charging EVs while driving, eliminating the need to stop the vehicle to charge the battery [1], [2], [3], [4], [5]. This solution, although very expensive because it involves the construction of important infrastructures such as electrified roads and lanes, overcomes the limits imposed by batteries in terms of EV range, making it widely extended and theoretically infinite [6], [7], [8]. By DWPT technology it is possible to limit the capacity of the on-board batteries, which can therefore be smaller and lighter, reducing costs and weight of the vehicle, but above all it is possible to eliminate stops for recharging the EV with undoubted advantages especially on long journeys. For this reason, the DWPT completes autonomous driving systems, making the EV autonomous with respect to the propellant since it is acquired along electrified roads.

Despite the attractiveness of DWPT systems related to the mentioned advantages, concerns regarding electromagnetic compatibility (EMC) and electromagnetic field (EMF) safety pose challenges to reducing magnetic field emissions associated with these systems [5], [9]. In many DWPT demonstrative projects [2], the compensation topology adopted is mostly series-series (SS) due to its simplicity. SS compensation is particularly advantageous in DWPT short-track architecture, where multiple transmitting coils are embedded in the electrified lane and are activated once at a time, only when a vehicle with a receiving coil, during its movement, passes above one of them. Since LCC compensation has been shown in previous studies [10], [11], [12] to be more effective at reducing magnetic field emissions [13], [14], its application in DWPT systems is here explored to mitigate EMC and EMF issues [10], [11], [12], [13], [14].

The associate editor coordinating the review of this manuscript and approving it for publication was Kai Song.

Mitigating the magnetic field in WPT systems is challenging because these systems operate at frequencies in the tens of kilohertz (e.g., $f = 85$ kHz for stationary light-duty vehicles according to SAE J2954 Standard [33], and for DWPT systems in the European Project Fabric [2]) where magnetic field penetration is high. Additionally, the magnetic field is essential for the efficient operation of the WPT system itself [15]. In the recent past, several research studies have investigated various mitigation strategies for WPT systems. Some of them have focused on the design of optimized shielding panels made of conductive and/or magnetic materials [15], [16]. The use of these materials significantly reduces the magnetic field in specific areas (e.g., inside the vehicle). However, due to the air gap between the transmitting and receiving coils, magnetic flux leakage remains significant, resulting in high magnetic field strengths mainly beside the vehicle.

Other mitigation techniques involve additional compensation loops, which can be reactive [17], [18], [19], [20], [21], [22], [23] (i.e., loop current induced by Faraday's Law) or active [24], [25], [26] (i.e., loop current produced by an independent source). The current flowing through these loops generates a magnetic field that opposes the incident field, thereby reducing the total field strength in certain areas. In any case, all these techniques require installing additional parts on the vehicle and/or along the electrified road section, with significant installation and maintenance costs.

Another solution is based on the reduction and/or redistribution of the coil currents using additional electronic units, typically buck or boost converters [27], [28], [29]. While this approach allows precise and real-time adjustable current and impedance tuning (and consequently magnetic field control), it comes with added costs, complexity, and increased losses.

Here, we present a method based on double sided LCC compensation which permits adjusting the current distribution between the ground assembly (GA) coil and the vehicle assembly (VA) coil, without requiring additional components on the vehicle or on the road. LCC compensation has been extensively analyzed by many researchers to enhance the electrical performance of wireless power transfer (WPT) systems and reduce stress on electronic units such as inverters and rectifiers. LCC compensation was also applied to stationary WPT systems to reduce magnetic field emissions [13], [14]. The results demonstrate the excellent performance of this solution; however, no guidelines are provided for optimizing the LCC network design.

A notable advancement from previous studies is presented here with the development of a new analytical method for selecting LCC network parameters. This method aims to minimize magnetic field strength in critical areas without altering the input impedance of the WPT system, thereby achieving a significant reduction in magnetic field emissions [5], [15].

II. DWPT SYSTEM

The DWPT system under consideration relies on resonant inductive coupling technology and features a short-track architecture. This setup entails a series of identical planar GA coils embedded in the road pavement, while a VA coil is positioned under the EV, as shown in Fig.1. GA coils, powered by a power electronic system, become active only when an EV is positioned directly above them during its movement. By appropriately selecting the size of the coils, it is possible to design a DWPT system wherein the GA coils are powered sequentially, one at a time.

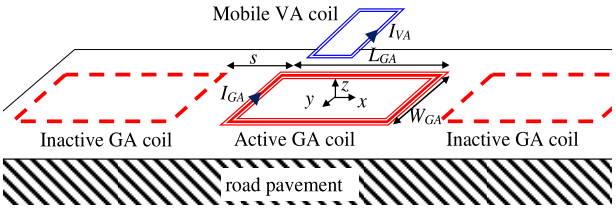

FIGURE 1. Configuration of DWPT coils with short-track architecture.

The DWPT configuration here adopted is derived from the European Project Fabric, operating at a frequency of 85 kHz and capable of transferring to the EV a maximum power of 10 kW [2]. The GA planar coils are rectangular, measuring $l_{GA} = 150$ cm by $w_{GA} = 50$ cm, and consist of $N_{GA} = 10$ turns. They are positioned at a separation distance along the road (x axis) $s = 30$ cm. The onboard VA coil is a 10-turn rectangular coil with external dimensions $l_{VA} = 40$ cm by $w_{VA} = 62$ cm. Two $15 \times 25 \times 0.5$ cm^3 ferrite blocks are positioned next to the VA coil [2]. The vertical separation between GA and VA coils is $\Delta z = 20$ cm. A Litz wire made up of 1260 AWG 38 insulated copper strands is used for the coils.

Even assuming a very high speed of 100 km/h ($= 27.78$ m/s) for a vehicle during wireless charging, the transit time τ over the 1.5 m long GA coil is approximately $\tau = 54$ ms. Compared to the time period of an 85 kHz wave, which is equal to $T = 1/f = 11.765$ μs, the transit time τ is much bigger than T (i.e., $\tau \gg T$). Therefore, it is evident that the electrical phenomenon is significantly faster than the kinematic one and the electrical system can be assumed to be stationary. This assumption holds particularly true for lower vehicle speeds. While the movement of the vehicle alters the mutual positions of the GA and VA coils, affecting the coupling factor k, the electrical phenomenon can still be modelled by a stationary circuit for each position of the coils. Assuming that the origin of the coordinate axes is the center of the active GA coil, the mutual position of the coils is defined by Δx, Δy, Δz which are the coordinates of the VA coil center, as shown in Fig. 2. Δx and Δy indicate the misalignment along the two axes in the xy plane, respectively, while Δz is the distance along the z axis. For perfectly aligned coils we have $\Delta x = 0$, $\Delta y = 0$, $\Delta z = 20$ cm. The coupling factor k depends on the separation distances between the centers of the GA and VA coils, $k = k(\Delta x, \Delta y, \Delta z)$.

The equivalent circuit of DWPT coils is shown in Fig.3, where the two coils are modeled by series resistances R_1 and R_2 and self-inductances L_1 and L_2, being subscripts 1 and 2 referred to GA and VA coils, respectively.

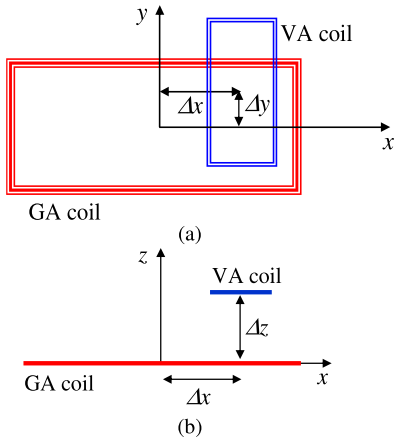

FIGURE 2. GA and VA coils on *xy* plane (i.e., top view) (a) and *xz* plane (i.e., lateral view) (b).

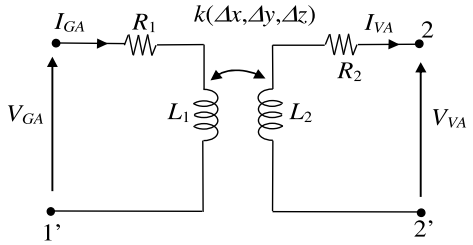

FIGURE 3. Equivalent circuit of two coupled coils where the coupling factor k depends on the coil reciprocal position, $k = k(\Delta x, \Delta y, \Delta z)$.

The inductive coupling between coils is modeled by the coupling factor k given by:

$$k\left(\Delta x, \Delta y, \Delta z\right) = \frac{M\left(\Delta x, \Delta y, \Delta z\right)}{\sqrt{L_1 L_2}} \tag{1}$$

being $M(\Delta x, \Delta y, \Delta z)$ the mutual inductance that depends on the mutual positions of the coils, while the self-inductances L_1 and L_2 remain almost constant.

III. MATHEMATICAL FORMULATION

A. MAGNETIC FIELD EMISSION

The magnetic flux density vector in phasor form, $\boldsymbol{B}= \boldsymbol{B}(\omega, \boldsymbol{r})$, depends on the angular frequency ω and position $\boldsymbol{r}$. It is produced by the phasor currents I_{GA} and I_{VA} flowing in the GA and VA coils, respectively, via Ampere's law. When neglecting non-linearities, the magnetic flux density can be calculated by superposition as follows:

$$\boldsymbol{B}\left(\omega, \boldsymbol{r}\right) = \boldsymbol{B}_{GA}\left(\omega, \boldsymbol{r}\right) + \boldsymbol{B}_{VA}\left(\omega, \boldsymbol{r}\right) \tag{2}$$

where $\boldsymbol{B}_{GA}$ and $\boldsymbol{B}_{VA}$ are the magnetic flux densities produced by coil phasor currents I_{GA} and I_{VA}, respectively.

The magnetic field distribution in a complex configuration as that of a DWPT system can be evaluated by solving the magneto quasi static (MQS) field equation in the frequency domain in terms of magnetic vector potential $\boldsymbol{A}$ and electric potential φ given by:

$$\nabla \times \frac{1}{\mu} \nabla \times \boldsymbol{A} + \sigma \left(j\omega \boldsymbol{A} + \nabla \phi\right) = \boldsymbol{J}_s \tag{3}$$

in combination with the continuity equation:

$$\nabla \cdot \left(-\sigma \left(j\omega \boldsymbol{A} + \nabla \phi\right) + \boldsymbol{J}_s\right) = 0 \tag{4}$$

where μ is the magnetic permeability, σ is the electrical conductivity and $\boldsymbol{J}_s$ is the current source density. The magnetic flux density $\boldsymbol{B}$, the magnetic field $\boldsymbol{H}$, the electric field $\boldsymbol{E}$, and the source current density $\boldsymbol{J}_s$ can be expressed in terms of potentials $\boldsymbol{A}$ and φ by

$$\boldsymbol{B} = \nabla \times \boldsymbol{A} \tag{5a}$$

$$\boldsymbol{H} = \frac{\nabla \times \boldsymbol{A}}{\mu} \tag{5b}$$

$$\boldsymbol{E} = -j\omega \boldsymbol{A} - \nabla \phi \tag{5c}$$

$$\boldsymbol{J} = -j\omega\sigma \boldsymbol{A} - \sigma \nabla \phi + \boldsymbol{J}_s \tag{5d}$$

The magnetic flux density $\boldsymbol{B}_{GA} = B_{GA}(\omega, \boldsymbol{r})$ in (2) can be evaluated by solving (3)-(5), imposing I_{GA} as magnetic field source, while I_{VA} is assumed to be zero. The magnetic flux density $\boldsymbol{B}_{VA} = B_{VA}(\omega, \boldsymbol{r})$ is calculated similarly, i.e., imposing I_{VA} to be the magnetic field source while $I_{GA} = 0$.

Equation (2) can be rewritten as

$$\boldsymbol{B}\left(\omega, r\right) = \boldsymbol{b}_{GA}\left(\omega, \boldsymbol{r}\right) I_{GA} + \boldsymbol{b}_{VA}\left(\omega, \boldsymbol{r}\right) I_{VA} \tag{6}$$

being $\boldsymbol{b}_{GA}(\omega, \boldsymbol{r}) = B_{GA}(\omega, \boldsymbol{r})$ when $I_{GA} = 1$ A and $I_{VA} = 0$, and $\boldsymbol{b}_{VA}(\omega, \boldsymbol{r}) = B_{VA}(\omega, \boldsymbol{r})$ when $I_{VA} = 1$ A and $I_{GA} = 0$. The complex vector transfer functions $\boldsymbol{b}_{GA}$ and $\boldsymbol{b}_{VA}$ are very useful because they simplify the analysis of the magnetic field for a given system configuration. This approach allows us to easily evaluate the magnetic field resulting from variations in the coil currents, such as those produced by adjustments in the compensation networks, without requiring any additional field simulation.

B. COMPENSATION OF A DWPT SYSTEM

As mentioned in the Introduction, the DWPT system operates in resonance conditions achieved by compensating the inductive reactance of the coils with additional circuit components (i.e., compensation networks) designed to provide a capacitive reactance. The simplest compensation networks are composed of capacitors connected in series with the coils, known as SS compensation. The equivalent circuit is shown in Fig. 4 where V_S and R_S represent the source, R_L the load, and the SS compensation capacitors C_1 and C_2 are given by:

$$C_1 = \frac{1}{\omega_0^2 L_1} \tag{7a}$$

$$C_2 = \frac{1}{\omega_0^2 L_2} \tag{7b}$$

being $\omega_0 = 2\pi f_0$ and f_0 the resonance frequency.

More complex compensation networks are based on multiple reactive components, leading to multi-resonant compensation. Among these, the most popular, owing to

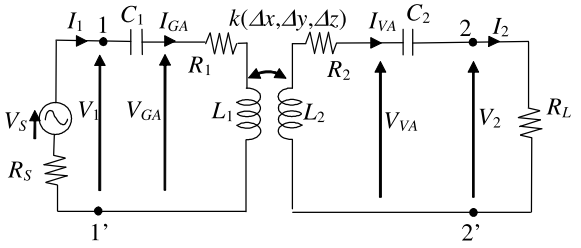

FIGURE 4. Equivalent circuit of a DWPT coil system with SS compensation and coupling factor $k = k(\Delta x, \Delta y, \Delta z)$.

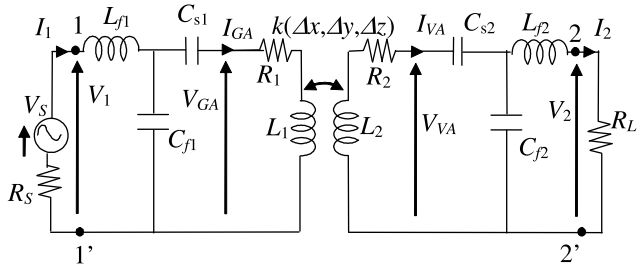

FIGURE 5. Equivalent circuit of a DWPT coil system with LCC compensation and coupling factor $k = k(\Delta x, \Delta y, \Delta z)$.

its efficiency, is the LCC compensation shown in Fig. 5. An LCC network includes one inductor and two additional capacitors. Double sided LCC compensation is modeled by L_{f1}, C_{f1}, C_{s1} for the GA and L_{f2}, C_{f2} and C_{s2} for the VA [13], [14]. Note that with LCC compensation the currents at the input port 1-1' and at the output port 2-2', denoted as I_1 and I_2 respectively, differ from I_{GA} and I_{VA}, which instead flow through the inductors L_1 and L_2 and which are the sources of the magnetic field.

In LCC compensation, the circuit parameters of the reactive components are related by the following formulas [5]:

$$L_{f1}\, C_{f1} = 1/\omega_0^2 \tag{8a}$$
$$L_{f2}\, C_{f2} = 1/\omega_0^2 \tag{8b}$$
$$L_1 - L_{f1} = 1/(\omega_0^2\, C_{s1}) \tag{8c}$$
$$L_2 - L_{f2} = 1/(\omega_0^2\, C_{s2}) \tag{8d}$$

The WPT performance depends on L_{f1} and L_{f2} which are selected based on the desired input and output voltage and current levels, output power and coupling factor. The primary side of the compensation networks permits to optimize the system for a given input voltage level while the secondary side is used to match the WPT coupler with the load. After selecting L_{f1} and L_{f2}, the values of capacitances C_{f1} and C_{f2} are determined from (8).

The power transfer efficiency η is given by the ratio between the real power P_2 at the output port 2-2' and the real power P_1 at the input port 1-1' as [5]:

$$\eta = \frac{P_2}{P_1} = \frac{real\left\{V_2 I_2^*\right\}}{real\left\{V_1 I_1^*\right\}} \tag{9}$$

or in terms of circuit parameters by [19]:

$$\eta = \frac{\omega_0^2 M\,(\Delta x,\, \Delta y,\, \Delta z)^2}{\left(1+\frac{R_2 R_L}{\omega_0^2 L_{f2}^2}\right)\left(R_1\left(R_2+\frac{\omega_0^2 L_{f2}^2}{R_L}\right)+\omega_0^2 M\,(\Delta x,\, \Delta y,\, \Delta z)^2\right)} \tag{10}$$

It means that varying the parameter L_{f2} it is possible to maximize the system efficiency and also vary the current gain α_I defined as [20]:

$$\alpha_I = \frac{I_{VA}}{I_{GA}} = \frac{j\omega_0 M\,(\Delta x,\, \Delta y,\, \Delta z)\, R_L}{R_2 R_L + \left(\omega_0 L_{f2}\right)^2} \tag{11}$$

The current flowing in the VA coil for LCC compensation at resonance is given by [5]:

$$I_{VA} = -\frac{R_L}{j\omega_0 L_{f2}} I_2 \tag{12}$$

C. MAGNETIC FIELD MITIGATION

The magnetic flux density in (6) can be expressed via (11) as:

$$\boldsymbol{B}\,(\omega, r) = \boldsymbol{b}_{GA}\,(\omega, \boldsymbol{r})\,\frac{I_{VA}}{\alpha_I} + \boldsymbol{b}_{VA}\,(\omega, \boldsymbol{r})\, I_{VA} \tag{13}$$

By substituting equations (12) into (13) the magnetic field can be expressed as:

$$\boldsymbol{B}\,(\omega, r) = -\left(\boldsymbol{b}_{GA}\,(\omega, \boldsymbol{r})\,\frac{1}{\alpha_I} + \boldsymbol{b}_{VA}\,(\omega, \boldsymbol{r})\right)\frac{R_L}{j\omega_0 L_{f2}} I_2 \tag{14}$$

and by substituting α_I as defined in (11) it yields:

$$\boldsymbol{B}\,(\omega, r) = -\left(\boldsymbol{b}_{GA}\,(\omega, \boldsymbol{r})\,\frac{R_2 R_L + \left(\omega_0 L_{f2}\right)^2}{j\omega_0 M\,(\Delta x,\, \Delta y,\, \Delta z)\, R_L} + \boldsymbol{b}_{VA}\,(\omega, \boldsymbol{r})\right) \cdot \frac{R_L}{j\omega_0 L_{f2}} I_2 \tag{15}$$

As can be seen from (15), the magnetic flux density depends only on the receiving side LCC compensation network (L_{f2}, and consequently C_{f2} and C_2) and the reciprocal position of the coils (M), since all other parameters (load resistance, coil resistance, load power, and frequency) are constants. Therefore, a value of L_{f2} can be found that minimizes (15), i.e., the magnetic field at a specific point. By applying this algorithm to a grid of points, it becomes possible to derive the spatial distribution of the magnetic field within a specified region. This procedure is highly valuable for ensuring compliance with EMF safety guidelines and EMC standards [9], [33], [34].The configuration that typically results in the worst-case scenario for magnetic field intensity occurs when the coupling factor is minimal, leading to significant magnetic flux leakage. This worst-case scenario serves as a reference for optimizing the LCC compensation network. The next section provides an analysis of how changes in network parameters affect system performance.

It is important to note that variations in secondary-side parameters of the LCC network can alter system behavior in terms of input impedance [5]. Specifically, the input impedance can be expressed as follows:

$$Z_{11'} = \left(\omega_0 L_{f1}\right)^2 \frac{1}{R_{GA} + \frac{\omega_0^2 M(\Delta x, \Delta y, \Delta z)^2 R_L}{R_{VA} R_L + \omega_0^2 L_{f2}^2}} \tag{16}$$

Equation (16) illustrates how the input impedance depends on both sides of the LCC network. Indeed, optimizing the parameters of the secondary-side LCC network to minimize magnetic field emissions will inevitably alter the input impedance and, consequently, the input voltage. However, maintaining a constant input voltage is crucial for the system's operation, as it is typically fixed. To achieve this, adjustments can be made on the primary side of the LCC network to restore the nominal input voltage. This adjustment does not compromise electrical efficiency or current distribution, as demonstrated in (10) and (11).

Fig. 6 shows the flow diagram of the proposed method. As a first step, the magnetic field produced by the WPT system is calculated in the most critical area beside the vehicle. The point (or cloud of points) where the magnetic field is maximum is selected to perform field mitigation. From this analysis the transfer functions $\boldsymbol{b}_{\mathbf{GA}}$ and $\boldsymbol{b}_{\mathbf{VA}}$ can be obtained. Then, by minimizing (14) or (15), the values L_{f2} that minimize the magnetic field are selected. Finally, an adjustment of the value L_{f1} in the primary side compensation network is performed to obtain the correct input impedance.

It is important to note that adjusting the current distribution between the GA and VA coils is not feasible adopting SS compensation because only a single value of the capacitors can be selected for each side to achieve resonance. Consequently, the magnetic field cannot be mitigated by modifying the compensation network parameters.

An alternative approach to adjusting impedance involves using electronic converters on both the transmitting and receiving sides of the SS compensated system [27], [28], [29]. However, this solution could increase costs, power losses, and system complexity compared to the proposed method, while the use of LCC compensation for magnetic field reduction is cost-effective and straightforward to implement in existing WPT systems. The losses introduced by LCC compensation are primarily due to the equivalent series resistance (ESR) of additional network components (L_{f1}, C_{f1}, L_{f2}, C_{f2}) which can be minimized by selecting suitable discrete components.

IV. NUMERICAL RESULTS

The proposed approach has been applied to a DWPT coil system with the Fabric configuration [2]. To reduce computational costs, the vehicle was not included in the calculations, but it was modeled by a metal mimic pan measuring 350×160 cm^2, with thickness $t = 2.5$ mm and electrical conductivity $\sigma = 37$ MS/m. In all tests, the output power is maintained at a constant value $P_2 = 10$ kW. The VA coil was assumed to be positioned in the center of the mimic pan.

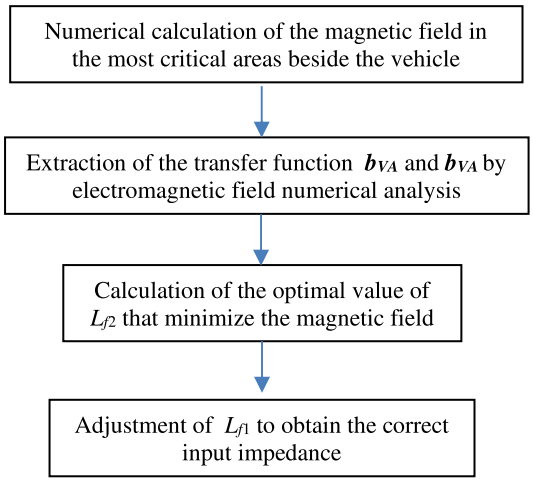

FIGURE 6. Flow diagram of the proposed method.

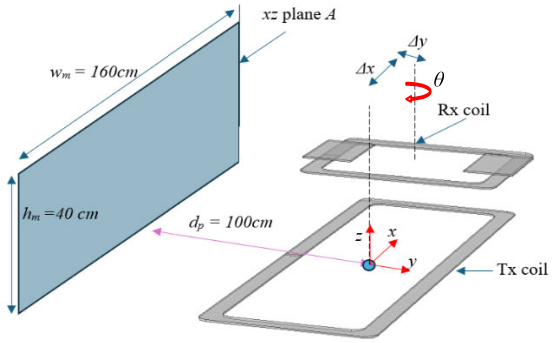

FIGURE 7. Equivalent circuit of a DWPT coil system with SS compensation and coupling factor $k = k(\Delta x, \Delta y, \Delta z)$.

As a first step, the coil parameters in terms of self and mutual inductances were calculated using the procedure described in [5]. This was done for different values of Δx (to simulate the movement of the vehicle) and Δy (to simulate lateral misalignment of the coils), while Δz was kept fixed at 20 cm.

A sketch of the configuration is shown in Fig.7 where the conductive mimic pan is not shown for clarity. The coil resistances have been obtained from the Litz wire datasheet, while the self-inductances and mutual inductance are extracted by 3D finite element method (FEM) simulations via the magnetic energy W_m solving the magneto-quasi static field equations [5]. The obtained circuit parameters of the WPT coils are shown in Table 1 while the coupling factor k obtained for different positions Δx, Δy of the VA coil is reported in Table 2. As can be seen, the worst case in terms of coupling factor k occurs with the maximum lateral misalignment, $\Delta x = 0$ and $\Delta y = 10$ cm.

The study examined how the reactive parameters of the LCC compensation network affect coil currents and power transfer efficiency η under the worst-case condition of minimal coupling factor ($k = 0.048$). Specifically, the impact of varying inductance L_{f2} (and consequently capacitance C_{f2} via (8b)) was analyzed. The calculated power

TABLE 1. Parameters of the DWPT system.

L_1 (μH)	L_2 (μH)	R_1 (mΩ)	R_2 (mΩ)	R_L (Ω)	P_2 (kW)
348	175	255	155	16	10

TABLE 2. Coupling factor to vary coil allignment.

Δx (cm)	Δy (cm)	Δz (cm)	*Coupling factor* $k(\Delta x,\Delta y,\Delta z)$
0	0	20	0.053
25	0	20	0.055
50	0	20	0.057
0	5	20	0.050
0	10	20	0.048
50	5	20	0.050
50	10	20	0.051

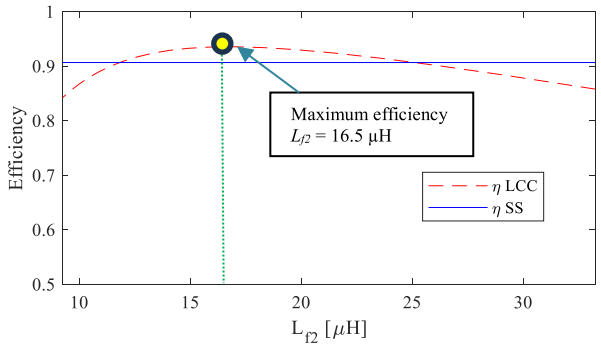

FIGURE 8. Power transfer efficiency η for SS compensation and for LCC compensation vs. parameter L_{f2}.

transfer efficiency η is shown in Fig. 8. Efficiency peaks at $L_{f2} = 16.5\ \mu$H, when an optimal match with the proposed load is obtained.

It is important to note that the efficiency achieved with LCC compensation slightly exceeds that of SS compensation, primarily due to better load matching capabilities. However, this finding is specific to the examined configuration and may not be applicable universally.

The coil currents I_{GA} and I_{VA} are shown in Fig. 9a (rms values) and Fig. 9b (phase shift between I_{GA} and I_{VA}). The variation of the receiving side parameters of the LCC compensation permits to adjust the gain α_I of the currents.

Next, attention was directed towards the magnetic field. The maximum magnetic field on the xz plane (denoted as A, see again to Fig. 7) for both SS compensation and LCC compensation was calculated. For each value of L_{f2} the magnetic field was computed using FEM simulation across the entire plane, and the maximum value was selected. The resulting graph is shown in Fig. 10.

As can be seen the variation of L_{f2}, and consequently the variation of the current gain α_I, has a very important impact on the maximum magnetic flux density, B_{max}. Assuming $L_{f2} = 14\ \mu$H, the maximum flux density B_{max} can be

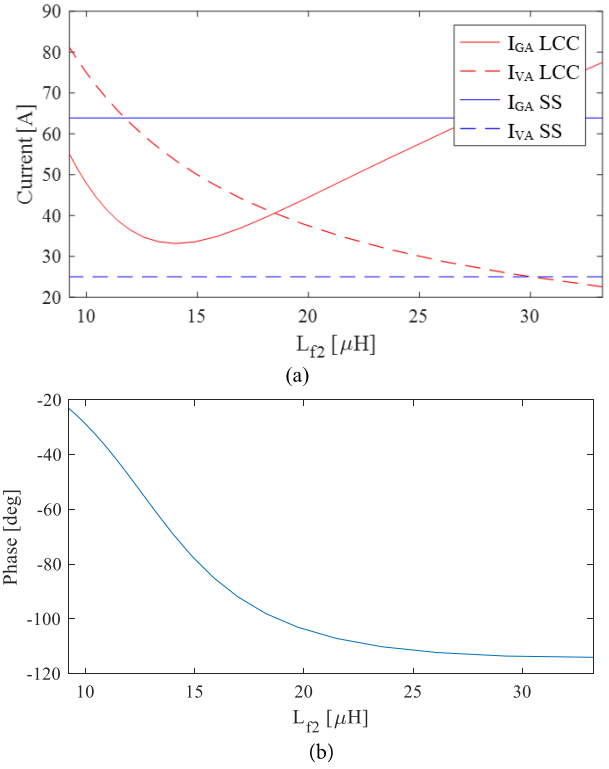

FIGURE 9. Coil currents I_{GA} and I_{VA} for SS and LCC compensations varying L_{f2}: (a) rms values; (b) phase shift between I_{GA} and I_{VA} in LCC compensation.

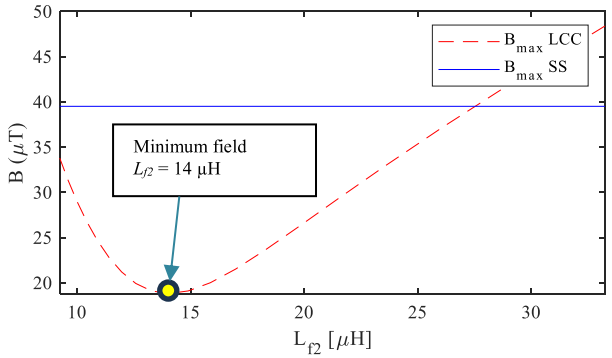

FIGURE 10. Maximum of the magnetic flux density, B_{max}, on plane A for SS compensation and for LCC compensation varying L_{f2}.

reduced by more than half compared to SS compensation. Moreover, compliance with the limit given by the ICNIRP 2010 guidelines (27μT@85kHz) is ensured [6]. The same value was obtained by minimizing equation (15) while considering the point on the plane where the magnetic field was at its maximum. It is noteworthy that the optimal reduction of the magnetic field occurs for a value of L_{f2} that differs from the one maximizing efficiency. Therefore, one can choose the appropriate value of L_{f2} to achieve the desired objective.

The maximum magnetic flux density B_{max} on the xz plane A for different vehicle positions Δx along the road, lateral misalignment Δy, and vehicle alignment θ respect the road in the case of LCC compensation, was also calculated.

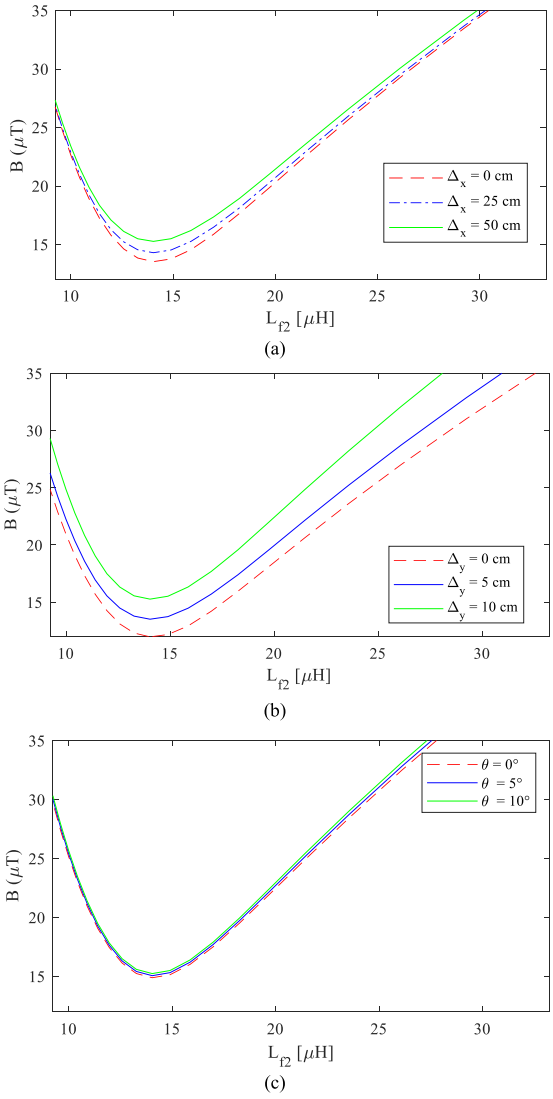

FIGURE 11. Maximum of the magnetic flux density, B_{max}, on plane *A* by varying the vehicle position Δx ($\Delta y = 10$ cm, $\theta = 0$) (a), vehicle position Δy ($\Delta x = 50$ cm, $\theta = 0$) and vehicle alignment θ ($\Delta y = 50$ cm, $\Delta y = 10$ cm) (c).

The results shown in Fig. 11 highlight that the vehicle position and inclination does not exert a significant influence on the selection of the optimal values for the secondary side LCC network. This is due to the minor variation of k during the vehicle's movement. Consequently, a dynamic adjustment of the parameter α_I is not necessary, and hence, the optimum value of L_{f2} remains essentially the same for all vehicle positions. Figure 12 shows the input voltage and system efficiency varying with L_{f1}. From this figure it is clear how the adjustment of the parameters of the primary side compensation network allows the selection of the desired input voltage without any influence on the efficiency of the system.

Finally, the calculated maps of the magnetic flux density B on the xz plane A(see again Fig. 7), considering two coil mutual positions (#1: $\Delta x = \Delta y = \theta = 0$; #2: $\Delta x = \Delta y = 10$ cm, $\theta = 0$), are shown in Figs. 13 and 14,

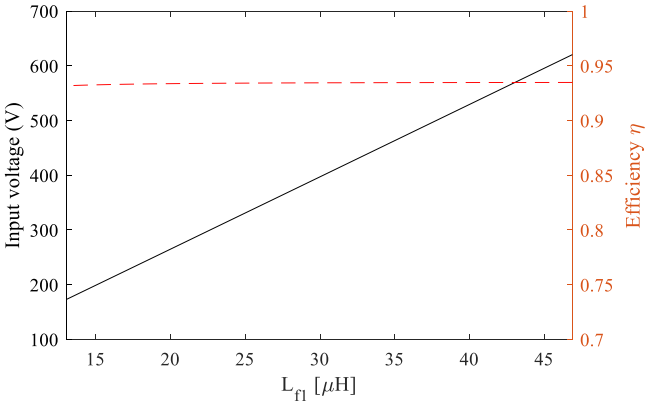

FIGURE 12. Input voltage (black line) and system efficiency (dotted red line) by varying L_{f1}.

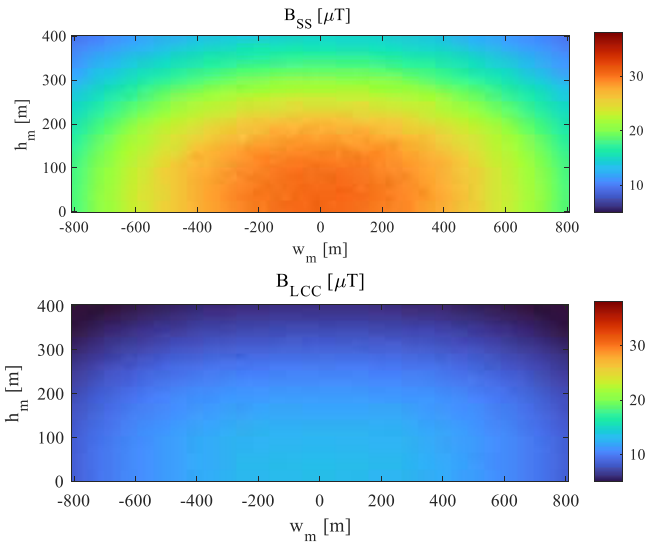

FIGURE 13. *B*-maps on plane *A* with SS and LCC compensation for $\Delta y = 0$ cm.

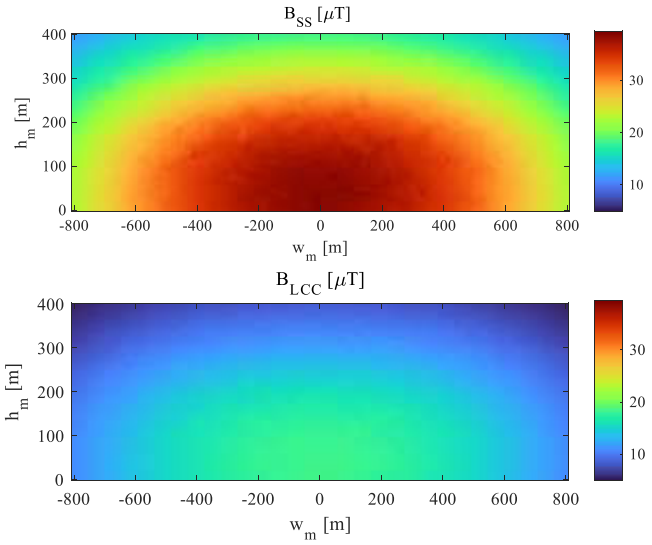

FIGURE 14. *B*-maps on plane *A* with SS and LCC compensation for $\Delta y = 10$ cm.

respectively, for SS compensation and LCC compensation with $L_{f2} = 14$ μH. As can be seen, the maximum magnetic flux density B_{max} with SS compensation exceeds the 27 μT reference level of the ICNIRP 2010 guidelines [6]. On the contrary, adopting LCC compensation with a suitable value of L_{f2}, the magnetic field reduction is significant and compliant with ICNIRP limit. It is worth noting that in the case under consideration, LCC compensation also enables an improvement in the electrical performance of the system, as it allows to match the DWPT system with both the source and load. However, under optimal load conditions, SS compensation can achieve higher efficiency due to the reduced number of passive components and consequently lower losses.

V. CONCLUSION

A method to mitigate the magnetic field produced by a DWPT system with LCC compensation on both transmitter and receiver was investigated. Initially, the proposed theory was presented, focusing on adjusting the secondary side LCC components to alter the current distribution between the coils. Guidelines for designing the LCC network were then defined to minimize the magnetic field at a specific point or in point clouds while maintaining the input impedance unchanged. Finally, the procedure was applied to a DWPT system using the coil configuration of the Fabric project. The results demonstrate that significant magnetic field reduction can be achieved using LCC compensation, without the need for additional components such as shielded panels or compensation coils on the vehicle or ground assemblies, and without altering the system's input voltage.

REFERENCES

[1] G. A. Covic and J. T. Boys, "Inductive power transfer," *Proc. IEEE*, vol. 101, no. 6, pp. 1276–1289, Jun. 2013.

[2] *FeAsiBility Analysis and Development of On-Road ChargIng Solutions for Future Electric VehiCles*. Accessed: Jun. 18, 2024. [Online]. Available: https://cordis.europa.eu/project/id/605405/reporting/en

[3] A. Ahmad, M. S. Alam, and R. Chabaan, "A comprehensive review of wireless charging technologies for electric vehicles," *IEEE Trans. Transport. Electrific.*, vol. 4, no. 1, pp. 38–63, Mar. 2018.

[4] V.-B. Vu, A. Ramezani, A. Triviño, J. M. González-González, N. B. Kadandani, M. Dahidah, V. Pickert, M. Narimani, and J. Aguado, "Operation of inductive charging systems under misalignment conditions: A review for electric vehicles," *IEEE Trans. Transport. Electrific.*, vol. 9, no. 1, pp. 1857–1887, Mar. 2023.

[5] M. Feliziani, T. Campi, S. Cruciani, and F. Maradei, *Wireless Power Transfer for E-Mobility*, 1st ed., Amsterdam, The Netherlands: Elsevier, 2023.

[6] M. Rehman, S. Mirsaeidi, N. M. Nor, M. A. Koondhar, M. A. A. M. Zainuri, Z. M. Alaas, E. Tag-Eldin, N. A. Ghamry, and M. M. R. Ahmed, "A review of inductive power transfer: Emphasis on performance parameters, compensation topologies and coil design aspects," *IEEE Access*, vol. 11, pp. 144978–145010, 2023.

[7] K. Song, Y. Lan, X. Zhang, J. Jiang, C. Sun, G. Yang, F. Yang, and H. Lan, "A review on interoperability of wireless charging systems for electric vehicles," *Energies*, vol. 16, no. 4, p. 1653, Feb. 2023.

[8] Y. Shanmugam, N. R, P. Vishnuram, M. Bajaj, K. M. AboRas, P. Thakur, and Kitmo, "A systematic review of dynamic wireless charging system for electric transportation," *IEEE Access*, vol. 10, pp. 133617–133642, 2022.

[9] J. Lin, "Guidelines for limiting exposure to time-varying electric and magnetic fields (1 Hz to 100 kHz)," *Health Phys.*, vol. 99, no. 6, pp. 818–836, Dec. 2010, doi: 10.1097/hp.0b013e3181f06c86.

[10] Z. Pantic, S. Bai, and S. M. Lukic, "ZCS *LCC*-compensated resonant inverter for inductive-power-transfer application," *IEEE Trans. Ind. Electron.*, vol. 58, no. 8, pp. 3500–3510, Aug. 2011.

[11] S. Li, W. Li, J. Deng, T. D. Nguyen, and C. C. Mi, "A double-sided LCC compensation network and its tuning method for wireless power transfer," *IEEE Trans. Veh. Technol.*, vol. 64, no. 6, pp. 2261–2273, Jun. 2015.

[12] M. Xiong, H. Dai, Q. Li, Z. Jiang, Z. Luo, and X. Wei, "Design of the LCC-SP topology with a current doubler for 11-kW wireless charging system of electric vehicles," *IEEE Trans. Transport. Electrific.*, vol. 7, no. 4, pp. 2128–2142, Dec. 2021.

[13] M. Feliziani, T. Campi, S. Cruciani, F. Maradei, U. Grasselli, M. Macellari, and L. Schirone, "Robust LCC compensation in wireless power transfer with variable coupling factor due to coil misalignment," in *Proc. IEEE 15th Int. Conf. Environ. Electr. Eng. (EEEIC)*, Rome, Rome, Italy, Jun. 2015, pp. 1181–1186.

[14] T. Campi, S. Cruciani, F. Maradei, and M. Feliziani, "Near-field reduction in a wireless power transfer system using LCC compensation," *IEEE Trans. Electromagn. Compat.*, vol. 59, no. 2, pp. 686–694, Apr. 2017.

[15] T. Campi, S. Cruciani, F. Maradei, and M. Feliziani, "Magnetic field during wireless charging in an electric vehicle according to standard SAE J2954," *Energies*, vol. 12, no. 9, p. 1795, May 2019.

[16] T. Campi, S. Cruciani, and M. Feliziani, "Magnetic shielding of wireless power transfer systems," in *Proc. Int. Symp. Electromagn. Compat.*, May 2014, pp. 422–425.

[17] J. Kim, J. Kim, S. Kong, H. Kim, I.-S. Suh, N. P. Suh, D.-H. Cho, J. Kim, and S. Ahn, "Coil design and shielding methods for a magnetic resonant wireless power transfer system," *Proc. IEEE*, vol. 101, no. 6, pp. 1332–1342, Jun. 2013.

[18] S. Kim, H.-H. Park, J. Kim, J. Kim, and S. Ahn, "Design and analysis of a resonant reactive shield for a wireless power electric vehicle," *IEEE Trans. Microwave Theory Techn.*, vol. 62, no. 4, pp. 1057–1066, Apr. 2014.

[19] M. Ishida and T. Watanabe, "Magnetic field canceling coil for wireless power transfer system," in *Proc. IEEE Wireless Power Transf. Conf. (WPTC)*, May 2015, pp. 1–4.

[20] H. Kim, C. Song, D.-H. Kim, D. H. Jung, I.-M. Kim, Y.-I. Kim, J. Kim, S. Ahn, and J. Kim, "Coil design and measurements of automotive magnetic resonant wireless charging system for high-efficiency and low magnetic field leakage," *IEEE Trans. Microw. Theory Techn.*, vol. 64, no. 2, pp. 383–400, Feb. 2016.

[21] J. Park, D. Kim, K. Hwang, H. H. Park, S. I. Kwak, J. H. Kwon, and S. Ahn, "A resonant reactive shielding for planar wireless power transfer system in smartphone application," *IEEE Trans. Electromagn. Compat.*, vol. 59, no. 2, pp. 695–703, Apr. 2017.

[22] Q. Zhu, Y. Zhang, Y. Guo, C. Liao, L. Wang, and L. Wang, "Null-coupled electromagnetic field canceling coil for wireless power transfer system," *IEEE Trans. Transport. Electrific.*, vol. 3, no. 2, pp. 464–473, Jun. 2017.

[23] M. Mohammad, E. T. Wodajo, S. Choi, and M. E. Elbuluk, "Modeling and design of passive shield to limit EMF emission and to minimize shield loss in unipolar wireless charging system for EV," *IEEE Trans. Power Electron.*, vol. 34, no. 12, pp. 12235–12245, Dec. 2019.

[24] S. Cruciani, T. Campi, F. Maradei, and M. Feliziani, "Active shielding applied to an electrified road in a dynamic wireless power transfer (WPT) system," *Energies*, vol. 13, no. 10, p. 2522, May 2020.

[25] T. Campi, S. Cruciani, F. Maradei, and M. Feliziani, "Magnetic field mitigation by multicoil active shielding in electric vehicles equipped with wireless power charging system," *IEEE Trans. Electromagn. Compat.*, vol. 62, no. 4, pp. 1398–1405, Aug. 2020.

[26] A. D. Scher, M. Mohammad, B. Ozpineci, and O. Onar, "Design and optimization of cancellation coil topologies for a ferrite-less wireless EV charging pad," in *Proc. IEEE Transport. Electrific. Conf. Expo. (ITEC)*, Chicago, IL, USA, Jun. 2021, pp. 1–7.

[27] Y. Yang, J. Wang, Z. Huang, I.-W. Iam, and C.-S. Lam, "Automatic containment of field exposure for roadway wireless electric vehicle charger," *IEEE Trans. Transport. Electrific.*, vol. 9, no. 3, pp. 1–17, Sep. 2023.

[28] T. Campi, S. Cruciani, V. De Santis, F. Maradei, and M. Feliziani, "EMC and EMF safety issues in wireless charging system for an electric vehicle (EV)," in *Proc. Int. Conf. Electr. Electron. Technol. Automot.*, Jun. 2017, pp. 1–4.

[29] Z. Miao, D. Liu, and C. Gong, "Efficiency enhancement for an inductive wireless power transfer system by optimizing the impedance matching networks," *IEEE Trans. Biomed. Circuits Syst.*, vol. 11, no. 5, pp. 1160–1170, Oct. 2017.

[30] Z. Lu, Y. Zhao, and D. Liu, "Adaptive impedance matching scheme for magnetic MIMO wireless power transfer system," *Electronics*, vol. 10, no. 22, p. 2788, Nov. 2021.
[31] H. He, S. Wang, Y. Liu, C. Jiang, X. Wu, B. Wei, and B. Jiang, "Maximum efficiency tracking for dynamic WPT system based on optimal input voltage matching," *IEEE Access*, vol. 8, pp. 215224–215234, 2020.
[32] L. Huang, A. P. Hu, A. K. Swain, and Y. Su, "Z-impedance compensation for wireless power transfer based on electric field," *IEEE Trans. Power Electron.*, vol. 31, no. 11, pp. 7556–7563, Nov. 2016.
[33] *Wireless Power Transfer for Light-Duty Plug-in/Electric Vehicles and Alignment Methodology*, document SAE J2954, 2022.
[34] *Active Implantable Medical Devices -Electromagnetic Compatibility EMC Test Protocols for Implantable Cardiac Pacemakers, Implantable Cardioverter Defibrillators and Cardiac Resynchronization Devices*, Standard ISO 14117, Int. Org. for Standardization, 2019.

TOMMASO CAMPI received the Laurea degree in telecommunication engineering and the Ph.D. degree in electrical engineering from the University of L'Aquila, L'Aquila, Italy, in 2014 and 2017, respectively. He is currently an Associate Professor with Sapienza University of Rome, Italy. His research interests include wireless power transfer and electromagnetic compatibility. He received the Best Paper Prize at the IEEE Conference on Electromagnetic Field Computation (CEFC), Annecy, France, in 2014; the Best Paper Award at the IEEE WPW 2019, Wireless Power Week, London, U.K., in 2019, IEEE CEFC 2018, 18th Biennial IEEE Conference on Electromagnetic Field Computation, Hangzhou, China, in 2019; and the Kanda Award for the most cited paper of IEEE TRANSACTIONS ON ELECTROMAGNETIC COMPATIBILITY in the past five years.

SILVANO CRUCIANI received the Laurea degree in information and automation engineering and the Ph.D. degree in electrical engineering from the University of L'Aquila, L'Aquila, Italy, in 2010 and 2015, respectively. He is currently a Researcher (RTD-b) with the Tor Vergata University of Rome. His main research interests include numerical methods, wireless power transfer, and EMF safety. He received the Best Paper Award at the IEEE WPW 2019, the Wireless Power Week, London, U.K., in 2019; and the Motohisa Kanda Award for the Most Cited (2015–2019) IEEE TRANSACTIONS ON ELECTROMAGNETIC COMPATIBILITY Paper.

FRANCESCA MARADEI (Senior Member, IEEE) received the Laurea degree (cum laude) in electrical engineering and the Ph.D. degree in electrical engineering from Sapienza University of Rome, in 1992 and 1997, respectively. In 1996, she joined the Department of Electrical Engineering, Sapienza University, where she is currently a Full Professor. She has authored more than 150 technical papers in the fields of computational electromagnetics, EMC, and wireless power transfer technology. She is a Life Member of the IEEE EMC Society and a member of the EMC Europe International Steering Committee. She received the 2015 Laurence Cumming Award for outstanding service to the IEEE EMC Society. She was the President of the IEEE Electromagnetic Compatibility Society, from 2010 to 2011, and an Associate Editor of IEEE TRANSACTIONS ON ELECTROMAGNETIC COMPATIBILITY, from 1999 to 2000.

MAURO FELIZIANI (Senior Member, IEEE) received the degree in electrical engineering from the University of Rome "La Sapienza," Rome, Italy, in 1983.

From 1987 to 1994, he was with the University of Rome "La Sapienza" as a Researcher (1987–1990), an Assistant Professor (1990–1992), and an Associate Professor (1992–1994). In 1994, he joined the University of L'Aquila, Italy, as a Full Professor of electrical engineering. He is the author or co-author of more than 180 papers published in the fields of electromagnetic compatibility (EMC) and electromagnetic field numerical computation. His current research interests include wireless power transfer and bioelectromagnetics. He received the Best Paper Award of IEEE TRANSACTIONS ON INDUSTRY APPLICATIONS-Electrostatics Process Committee, in 1995; the Best Paper Award–EMC Europe 2000, Bruges, the Best Paper Prize–IEEE Conference on Electromagnetic Field Computation (CEFC), Annecy, France, in 2014; the Best Paper Award from the IEEE WPW 2019, Wireless Power Week, London, U.K., in 2019; and the 2019 Kanda Award for the most cited paper of IEEE TRANSACTIONS ON ELECTROMAGNETIC COMPATIBILITY, in the past five years. In 1994, he was a Co-Founder of the EMC Europe Symposium. He was the General Chair of the EMC Europe Symposium, Sorrento, Italy, in 2002, and the EMC Europe Workshop, Rome, in 2005. He was the Technical Program Committee Chair of EMC Europe 2012, Rome; the Chair of the International Steering Committee of the EMC Europe Symposium, from 2012 to 2015; and the Co-Chair of the EMC Europe Virtual Symposium 2020.

Open Access funding provided by 'Università degli Studi di Roma ''La Sapienza'' 2' within the CRUI CARE Agreement